PCCP

Accepted Manuscript

ROYAL SOCIETY OF CHEMISTRY

www.rsc.org/pccp

Revised Manuscript

Well-aligned Nd-doped SnO_2 nanorods layered array: preparation, characterization and enhanced alcohol-gas sensing performance

Guohui Qin[a], Fan Gao[a], Qiuping Jiang[a], Yuehua Li[*,b], Yongjun Liu[c], Li Luo[a], Kang Zhao[a], Heyun Zhao[*,a,d]

[a] *Department of Materials Science and Engineering, Yunnan University, Number 2 Green Lake North Road, Kunming, 650091, PR China.*

[b] *Advanced Analysis and Measurement Center of Dali University, number 2 Hongsheng Road, Dali, 671200, PR China.*

[c] *Advanced Analysis and Measurement Center of Yunnan University, Number 2 Green Lake North Road, Kunming, 650091, PR China.*

[d] *Yunnan Key Laboratory for Micro/Nano Materials and Technology, Yunnan University, Number 2 Green Lake North Road, Kunming 650091, P.R. China*

* *Corresponding author email: hyzhao@ynu.edu.cn (h.zhao); Tel: +86-871-5031124, Fax: +86-871-5153832; loneman2@163.com.*

Well-oriented Neodymium doped SnO_2 layered nanorods arrays were synthesized by a substrate-free hydrothermal route of using sodium stannate and sodium hydroxide at 210 °C. The morphology and phase structure of the Nd-doped SnO_2 nanoarrays were investigated by X-ray powder diffraction spectra, scanning electron microscopy, transmission electron microscopy, Raman scattering spectroscopy, X-ray photoelectron spectrum and BET method. The results demonstrated that the Nd-doped SnO_2 layered nanorods array showed a unique nanostructure combined together with double layered arrays of nanorods with a diameter of 12 nm and length of several hundred nanometers. The Nd-doped layered SnO_2 nanoarrays kept the crystal structure of the bulk SnO_2 and possessed more surface defects caused by the Nd ions doped into the SnO_2 lattice. The Nd dopant act as a crystallite growth inhibitor to prevent the SnO_2 nanorods growth up. An investigation into the gas-sensing properties indicated that the optimized doping level of 3.0 at% Nd-doped SnO_2 layered nanorods arrays exhibited an excellent sensing response toward alcohol at a lower temperature of 260 °C. The enhanced sensor performance was attributed to the higher specific surface area, multi-defect surface structure and the excellent catalytic properties of Nd dopant that is able to increase the amount of active sites on the surface of semiconducting oxides. The Nd-doped SnO_2 nanoarrays sensors were considered to be a promising candidate for trace alcohol detections in environmental gas monitor.

1. Introduction

Rutile structured tin oxide (SnO_2), as one of an important n-type semiconductor metal-oxide with a large direct energy band gap (E_g=3.6 eV, at 300 K) has gained prominent attention due to its extensive applications in many fields, such as Li ion batteries,[1] dye-sensitive solar cells,[2] field-effect transistors,[3] photocatalysis[4] and especially gas sensors.[5,6] Since the discovery of SnO_2 nanobelts in 2001,[7] one-dimensional (1D) nanostructures of SnO_2 such as rods, wires, tubes and belts have been attracting a great deal of interest for scientific research due to their unique properties and potential to revolutionize broad areas of nanotechnology.[8] However, these products are usually randomly oriented and difficult to be made into nanostructured devices to effectively play its performance advantages. Up to now, many efforts have been focused on the assembly and integration of nanorods/nanowires as building blocks into three-dimensional arrays for enhancing their performances and expanding their practical applications, including microelectronic devices, chemical and biological sensors, energy conversion and storage, light-emitting displays, and catalysis.[9,10] In recent years, a few 1-D SnO_2 nanoarrays with several different morphologies have already been synthesized by conventional growth of chemical vapor deposition (CVD),[11] thermal evaporation (TE),[12] hydrothermal approach[13] and so on. Although various physical and chemical routes have been developed to fabricate nanoarrays, these strategies need multiple steps, rigorous equipments or toxic reagents that limit their application. Especially, these methods always involve harsh, costly growth substrates such as Si, ITO, SiO_2, TiO_2, FTO, metal or alloy substrates, which affect the performance of the materials owing to the chemical stability, conductivity and toughness. Thus, it is still a tremendous challenge to develop a facile, effective, solution based, shape-controlled self-assembly method to realize the formation of complex aligned 1-D SnO_2 arrays without substrates, which will overcome the drawbacks or problems associated with substrates.

Volatile organic compound vapors (VOCs) such as alcohol, acetone, isopropanol, formaldehyde and so on, are the primary sources of indoor environmental pollutants and are considered seriously harmful to the human body.[14,15] There are notable correlations between VOCs emissions and different kinds of human health. In recent years, the investigation of gas sensor have received considerable attention for the profound influence on personal safety and detection of pollutants, toxins, and the transportation industries. SnO_2 is a well-known substance used for detection of different VOC pollutants owing to its low cost, high sensitivity, and quick gas response and thermal stability,[16] which has been extensively studied for detection of a wide variety of inflammable and toxic VOCs gases such as alcohol.[17] To date, there has been a great deal of research toward the development of miniaturized and highly efficient gas-sensing devices and their enhancement of sensor performance to detect various VOCs.

Many factors such as additives, grain size, microstructures and morphologies may influence the sensing properties of gas sensor significantly.[18] In order to improve the gas-sensing performances, nanostructured semiconductor oxides are attracting a great deal of attention due to their exclusive properties and novel applications. Many low dimensional nanostructures such as nanowires,[19] nanobelts,[20] nanorods,[21] nanotubes,[22] nanofibers and hierarchical flowerlike nanostructures,[23,24] have been found to show excellent sensing performances due to their high surface–volume ratio, abundant surface states and enhanced surface reactivity. Among them, attributing to their inherent high surface-to-volume ratio and ordered arrangement that is of great benefit for gas diffusion and mass transports in sensor materials, one-dimensional (1-D) nanoarray structures are preferable for the detection of pollutant gases.[25-27] Moreover, another simple and effective artifice to improve the sensor response is doping noble metals,[28,29] or rare earth metal.[30] Rare earth doped compounds have been studied because of their fast oxygen ion mobility and catalytic properties which are important factors in chemical sensing.[18] The effects of doping of Yb,[30] Pr,[31] La,[32] Ce,[33] and Sm[34] have been reported by various authors, indicating positive effect on gas sensing of nanomaterials. Although seldom research works have been also presented that Nd doping can enhance the sensing properties,[35-37] the effects of Nd doping on the sensing of VOCs gases, such as alcohol, however, remained unclear. In addition, to the best of our knowledge, no attention has yet been focused on the fabrication of Nd-doped SnO_2 well-aligned nanorarrays and their gas sensitive properties. So it is necessary to explore the preparation and the gas-sensing properties of Nd-doped SnO_2 well-aligned nanorarrays to reveal the potential applications for high performance sensor.

In the present work, pristine and different atomic ratios of Nd-doped well-aligned layered SnO_2 nanorod arrays were successfully synthesized using a substrate-free hydrothermal route without any surfactants. The gas sensing experiments of Nd-doped SnO_2 towards alcohol were carried out compared with the pristine SnO_2 nanoarrays to envisage the effect of Nd-doped on sensitivity, response and recovery times and selectivity, which reveal the potential applications for high performance sensor to detect alcohol in environmental gas monitor. A possible sensing mechanism of enhanced alcohol-gas sensing performance was also discussed for the Nd-doped SnO_2 nanorod arrays.

2. Experimental

2.1 Preparation of Nd-Doped layered SnO_2 nanoarrays

Pristine and Nd-doped SnO_2 layered nanoarrays were synthesized via a simple hydrothermal route without any surfactants and in the absence of substrates. For the synthesis of SnO_2 layered nanoarrays, sodium stannate trihydrate sodium stannate four-hydrate ($Na_2SnO_3·4H_2O$), neodymium chloride ($NdCl_3·6H_2O$), sodium hydroxide (NaOH) and absolute alcohol (C_2H_5OH) were used as precursors without further purification. All the used chemicals are highly pure and analytical grade reagents obtained from Sinopharm Chemical Reagent Co. (Shanghai, China). Deionized water was used throughout the experiments. Typically, the sodium stannate four-hydrate ($Na_2SnO_3·4H_2O$, 0.188 mmol) was dissolved in 20 ml distilled water with vigorous stirring for 30 min to form uniform solutions. In order to study the effect of Neodymium dopant on the sensing performance, a suitable amount of Neodymium chloride was added to the solution with Nd to Sn atomic ratio of 0 at%, 0.5 at%, 1 at% and 3 at%, respectively. At the same tine, the sodium hydroxide (NaOH, 7 mmol) was also dissolved in 20 ml distilled water with vigorous stirring for 30 min. Then, the obtained mixture suspension of $Na_2SnO_3·4H_2O$ and $NdCl_3·6H_2O$ was slowly dripped into the NaOH solution with ceaseless stirring kept at 40 ^oC for 30 min, forming a semitransparent colloidal solution. After that, 40 ml of absolute alcohol was gradually added into the above mixed solution with vigorous stirring for 60 min. The resulting white homogeneous suspension was transferred to a 100 ml Teflon-lined stainless steel autoclave and then heated in an oven at 210 °C for 48 h. After the autoclave cooled down naturally, a large amount of a greyish white precipitate was collected and washed several times with deionized water and absolute alcohol. Finally, the resulting products were dried in an oven at 80 °C for 24 h for further characterization.

2.2 Characterization

The crystal structure of layered SnO_2 nanoarrays were determined by powder X-ray diffraction. XRD patterns were recorded on a Rigaku D/MAX-3B powder diffractometer with copper target and K_α radiation (λ = 1.54056 Å) operated at 40 kV and 30 mA in the wide angle region from 15° to 90° (2θ) in steps of 0.02°. The morphologies of as-prepared layered SnO_2 nanoarrays films were investigated with a Quanta 200 FEG environmental scanning electron microscopy (ESEM) at an accelerating voltage of 25 kV, while performing detailed structural characterizations with a transmission electron microscope (TEM, JEOL 2010, 200 kV) equipped with selected area electron diffraction (SAED) pattern capabilities. The topological features and the composition of Sn, O, and Nd were determined by energy dispersive X-ray spectrometer on K and L lines. Raman scattering spectra were obtained using a Renishaw INVIA Laser Micro-Raman spectrometer. X-ray photoelectron spectroscopy (XPS) was recorded at room temperature in PHl X-tool. During XPS analysis, Al *Ka* X-ray beam was adopted as the excitation source and power was set to 250 W. UV/Vis measurements were made with a UV-2401PC spectrophotometer. The specific surface area of the product was determined by Brunauer-Emmett-Teller (BET) equation based on the nitrogen adsorption isotherm obtained with a Micromeritics Gemini VII apparatus (Surface Area and Porosity System), and the pore-size distribution was obtained from the desorption branch of the isotherm using the corrected form of the Kelvin equation by means of the Barrett-Joyner-Halenda (BJH) method.

2.3 Fabrication and gas-sensing performance tests

A series of sensors were elected indirect-heating structure as our previous detailed description of the sensor fabrication and gas detected.[27] A proper amount of the prepared sample was slightly ground together with several drops of water in an agate mortar to form a homogeneous paste. Then the paste was coated onto an alumina tube with Au electrodes and platinum wires which were used as electrical contacts. A Ni–Cr alloy coil was inserted through the tube as a heater to adjust the operating temperature from room temperature to 600 °C, which were controlled by tuning heating voltage. Before measuring the gas sensing properties, the gas sensors were aged at 500 °C for 120 h in dry air.

Gas-sensing properties test was performed on a JF02F gas sensing measurement system (Jin Feng Electronics of Sino-Platinum Metals Co. Ltd., China), which is a static system using atmospheric air as the interference gas and the diluting gas to obtain desired concentrations of target gases in a test chamber (about 15 L in volume). The export signal of the sensor was measured by using a conventional circuit in which the element was connected with an external resistor inseries at a circuit voltage. The target gas was injected into the chamber and the response of sensors began. The gas-sensing properties were assessed through sensor response S, which was defined as the ratio of R_a/R_g, where R_a and R_g stand for the electrical resistance of the sensor in atmospheric air and in the target gas, respectively. All of the tests in gas-sensing properties were performed at a relative humidity range of 50–70%.

3. Results and discussion

3.1 Characterization of Nd-doped SnO_2 nanoarray

X-ray powder diffraction (XRD) was used to characterize the crystal structure and composition of the products and corresponding the typical XRD patterns as shown in Fig. 1 depicted a substantial texture effect in accordance with the crystal shape anisotropy and orientation. All the available reflections of the present XRD phases have been fitted with a Gaussian distribution. For the pristine SnO_2 nanoarrays samples, all the diffraction peaks can be indexed to the rutile structured SnO_2 (tetragonal, space group P42/mnm (136), with tetragonal lattice parameters of a=b=4.738 Å, c=3.186 Å), which match well with the standard data file of SnO_2 crystal (JCPDS file No. 41-1445). No signals of secondary phase such as $Sn(OH)_4$ or SnO are found in the product, indicating that only SnO_2 with good crystallinity and purity were obtained under these conditions. For the 0.5 at% and 1 at% Nd-doped SnO_2 nanoarrays samples, the diffraction peaks are almost similar to that of the pristine SnO_2, no secondary phase is also found. Therefore, it can be speculated that Nd-oxides formed Nd-Sn-O solid solution with SnO_2 because no other species existed in Nd-doped SnO_2 samples. It is possible for Nd^{3+} ions cooperate with the matrix of SnO_2 particles to form Nd-Sn-O solid solution since the radius of Nd^{3+} (0.0983 nm) is not much bigger than that of Sn^{4+} (0.069 nm). However, for the 3 at% Nd-doped SnO_2 nanoarrays sample, two weak additional diffraction peaks corresponding to the position 28.6^o and 40.37^o can be observed in the XRD pattern curve d, indicating the presence of a secondary phase, which could be assigned to the crystalline phases of $Nd_2Sn_2O_7$ (JCPDS file No. 13-0185). This may be derived from that the 3 at% Nd doping is over the SnO_2 saturation, and the excess Nd atom reaction with the SnO_2 to form the new phase of $Nd_2Sn_2O_7$, which detected in the XRD measurement. Moreover, attention to the value of the relative intensities of all the SnO_2 layered nanoarray samples shown in Fig. 1 are distinct from that of SnO_2 powders, and higher intensity ratios of (101) and (002) to other planes in comparison with those in JCPDS file No.41-1445 are observed. The intensity of peak (002) of all the SnO_2 layered nanoarray samples enhance very significantly, which can be attributed to the oriented growth in the [001] direction and orient perfectly with their c-axis.[38] This result indicates that all SnO_2 nanoarray samples showed higher orientation.

The enlarged image of the diffraction peak corresponding to (110) plane of SnO_2 array nanocrystals between 25^o and 28^o was shown in Fig. 1b, which is used to observe the Nd doping effect on peak position and peak intensity. Fig. 1b shows the variation of peak intensity and full-width at half maximum (FWHM) as a function of Nd concentration from 0 at% to 3 at% along (110) plane. With increasing Nd contents, the peak position slightly shifted a angles $\Delta 2\theta$ ($\Delta 2\theta \sim 0.18^o$) towards lower side is observed, indicating an increase of the lattice parameter due to tensile/compressive stress on the lattice derived from the rare earth incorporation. This physical process suggests that a portion of the metal-oxide ions formed stable solid solution with SnO_2 and the metal-oxide ions occupy the regular lattice site in SnO_2.[18] The intensity of the peaks decrease and the full-width at half maximum (FWHM) of Nd-doped SnO_2 peaks increase with the increase of the Nd contents, betokening that the crystallite size decreases gradually with increasing Nd content. The crystallite size with respect to Nd dopant concentration was calculated using Scherer's Eq. (1)

$$D = \frac{k\lambda}{\beta \cos\theta} \tag{1}$$

Where k is a constant value taken as 0.89; λ is the wavelength of the X-ray source which taken as 1.5406 Å; β is the full width at half maximum (FWHM) and θ is the Bragg angle. By using Scherer's formula, the mean crystalline sizes of the obtained layered SnO_2 nanoarray samples are calculated to be about 27.3, 20.1, 16.4, 12.8 nm respectively, employing XRD data of the (110) plane diffraction peak. The results indicate that smaller and less ordered crystals are formed in the case of Nd-doped samples. The decrease of the crystallite size with the addition of Nd dopants suggests that the 3 at% of Nd dopant might lead to supersaturation which is responsible for the grain's shrinkage.[39] Since the ionic radius of Nd^{3+} (0.0983 nm) is larger than the ionic radius of Sn^{4+} (0.069 nm), incorporating Nd^{3+} ions into the matrix leads most likely to some distortion and stress in the cell and the lattice, respectively. As a consequence, the grains might break which causes a decrease in the crystallite size with respect to the Nd addition.

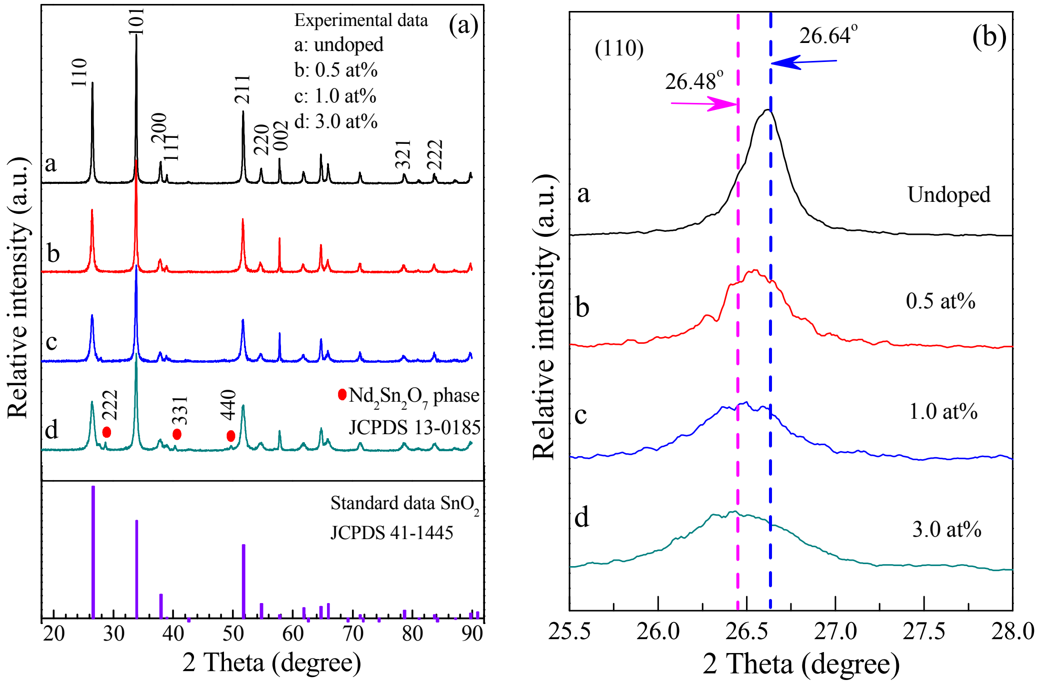

Fig. 1 (a) XRD patterns of Nd-doped SnO_2 layered nanorods array samples. (b) Comparison the shift of (110) peaks.

The morphology of as-prepared Nd-doped SnO_2 layered nanoarrays characterized by SEM. Fig. 2 shows the morphology of the as-prepared 0 at%, 1 at% and 3 at% Nd-doped layered SnO_2 nanoarray, respectaly. As shown in Fig. 2a, c and e, top-view images of layered SnO_2 nanorods array display large-area continuous, high ordered dense nanorods array. For our three layered SnO_2 nanorods array samples, the narrow size distribution of these nanorods with a fine round bar cross section as well as the vertical and dense alignment in the array is clearly observed. The nanorods density in the plane of the 1 at% and 3 at% Nd-doped layered SnO_2 nanoarray nanorods statistically counted to be *ca*. 258 and 283 μm^{-2} (Fig. 2a and c), and the width of the cross section was estimated approximately 18.2 and 12.6 nm. Fig. 2e displays the top-view image of the pristine SnO_2 nanorods array. By the same way, the nanorods density on the plane statistically counted to be *ca*. 223 μm^{-2}, and the width of the cross section was estimated approximately 29 nm. It is obvious that the diameter of the nanorods is thicker than that of Nd-doped nanorods of SnO_2 nanarrays synthesized under the same conditions, suggesting that the Nd dopant can act as a crystallite growth inhibitor for the SnO_2 material to prevent the nanorods further growth up.[40] This is in accordance with the result of the XRD patterns from Fig. 1. The small crystallite sized SnO_2 nanorods should provide a large surface area that could increase the probability of surface trapping, which enhence the sensitivity to the surface reaction.

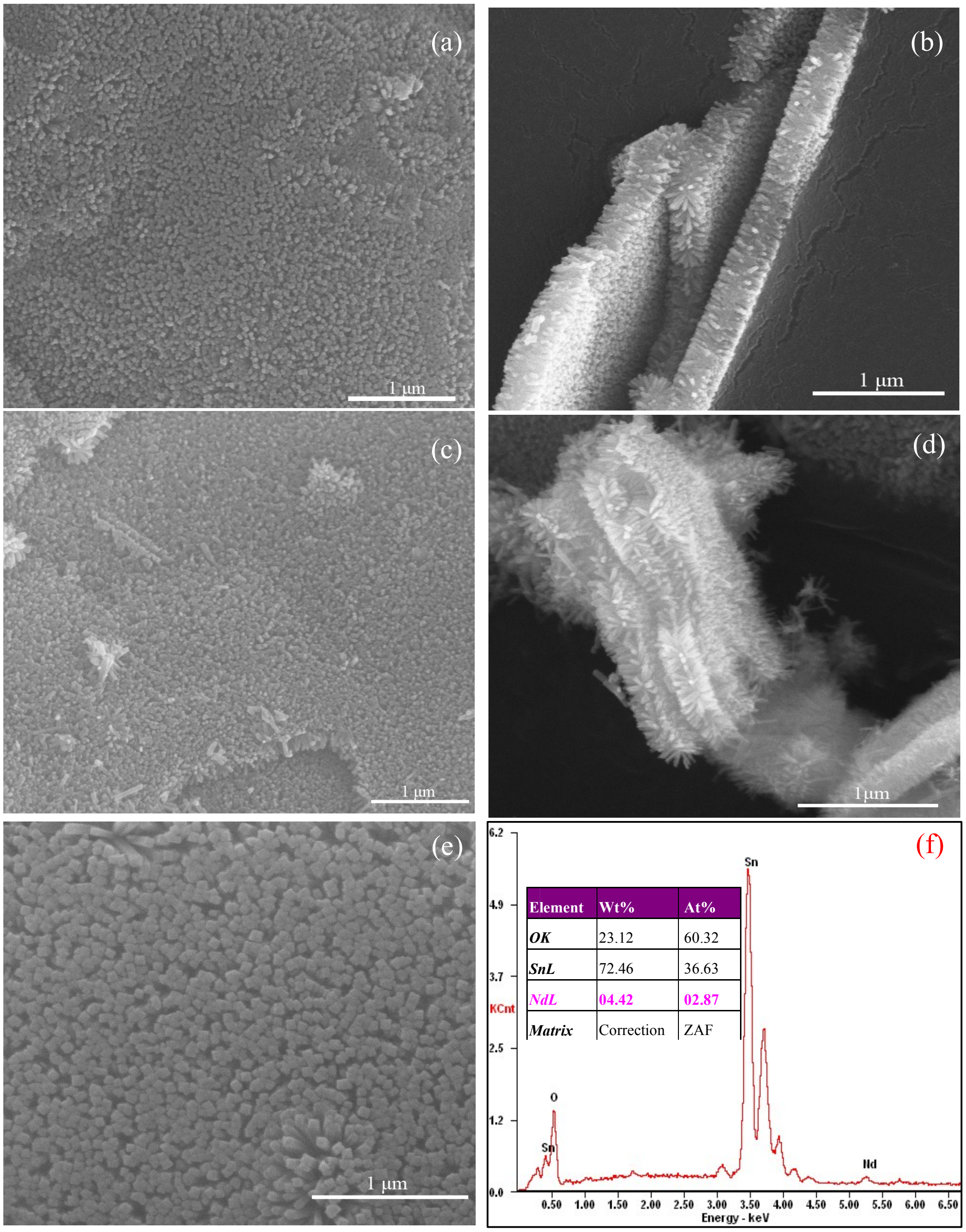

Element	Wt%	At%
OK	23.12	60.32
SnL	72.46	36.63
NdL	04.42	02.87
Matrix	Correction	ZAF

Fig. 2 (a) and (b) Top-view and Cross-sectional SEM image of 1 at% Nd-doped SnO_2 nanorods array. (c) and (d) Top-view and Cross-sectional SEM image of 3.0 at% Nd-doped SnO_2 nanorods array. (e) Pristine SnO_2 nanorods array SEM image (e) EDX spectrum of 3.0 at% Nd-doped SnO_2 nanorods array.

A section edge of the Nd-doped layered SnO_2 nanoarray as shown in Fig. 2b and d displays the small nanorods tightly combined together, and these nanorods are generally perpendicular and arranged in very large uniform arrays. It can be seen that Nd-doped layered SnO_2 nanoarray was tightly combined together by two parts of the nanrods array with an apparent interface in the centre. Each of the nanorods has one end outside with neatly arranged, exhibiting peculiar orderly arrayed structures. The nanorods on each part, growing approximately perpendicular to the interface, has a length of about 200–300 nm. Note that we did not use any substrate before reaction, which is usually employed for the growth of SnO_2 nanoarrays.[11,12] The EDX spectrum is used to confirm the composition of the samples. The typical EDX pattern of 3 at% Nd-doped layered SnO_2 nanorods array was presented in Fig. 2f. The quantitative atomic percentages of the compositional elements such as stannum (Sn), oxygen (O) and neodymium (Nd) were presented as an inset in Fig. 2f. The image shows the presence of Sn, Nd and O as the only elementary species in the SnO_2 sample. The EDX spectra showing the 2.87 at% of Nd content in SnO_2 nanoarray is consistent with the initial ratio of experimental design within the experimental error.

In order to further observe the morphology and microstructures of the products in detail, TEM, selected area electron diffraction (SAED) and HRTEM images of the 3 at% Nd-doped layered SnO_2 nanoarrays were shown in Fig. 3. Fig. 3a depicts a low-magnification TEM image of a section removed from the Nd-doped SnO_2 nanorods array assemblies, where the rods-like array nanostructure of the prepared SnO_2 nanorods array assemblies can be clearly seen. An enlarge peaked top TEM image of SnO_2 nanorods array shown in Fig. 3b confirms the product mainly consists of solid rod-like structure with a smooth surface and an obtuse angle top rather than a flat top. The straight nanorods have uniform diameters of around 12 nm, being in accordance with the SEM results. To get more detailed structure information about the construction units of the SnO_2 nanoarrays, HRTEM and FFT of an individual nanorod taken from the product after ultrasonication were carried out. Fig. 3c shows a high-resolution transmission electron micrograph (HRTEM) of a single SnO_2 nanorod and clear lattice fringes. Although the overview of HRTEM image illustrates that the single SnO_2 nanorod is of a high quality single rutile crystals, it is obvious that the overall structure of SnO_2 nanorod is not uniform. Here, in order to facilitate the description, we marked them as area A, B and C shown in Fig. 3c and d. As shown in the upper-left inset of Fig. 3c, an enlarge HRTEM image of the marked area A depicts a uniform structure and reveals 0.348 nm space between two adjacent lattice fringes parallel to the length of the nanorod, which is significantly larger than the usual value of 0.3347 nm of a bulk SnO_2. The space corresponds to the (110) lattice planes of SnO_2 in tetragonal cassiterite structure, indicating that the exposed facet of the SnO_2 nanorods is the (110) plane and the oriented growth is preferentially along the [001] direction.[41] The corresponding fast Fourier transform (FFT) shown in the lower-left inset of Fig. 3c is an agreement with the survey results of HRTEM. The enlarge HRTEM images of the marked area B and C shown in the upper-left inset of Fig. 3d depict the lattice fringes and reveals approximate 0.349 nm space between two adjacent lattice fringes, which also corresponds to the (110) lattice planes of SnO_2 in tetragonal cassiterite structure. However, it is obvious that lattice fringes in area B and C of SnO_2 nanorod are distorted and discohered, indicating dislocations and extended defects inside. The reason for this result is mainly originated in the ionic radius of Nd^{3+} is larger than the ionic radius of Sn^{4+}, incorporating Nd^{3+} ions into the matrix leads most likely to some distortion and stress in the cell and the lattice. As a result, the lattice fringes of SnO_2 nanorod might be distorted and discohered in the crystallite with respect to the Nd addition. These results support the XRD observation as shown in Fig. 1b.

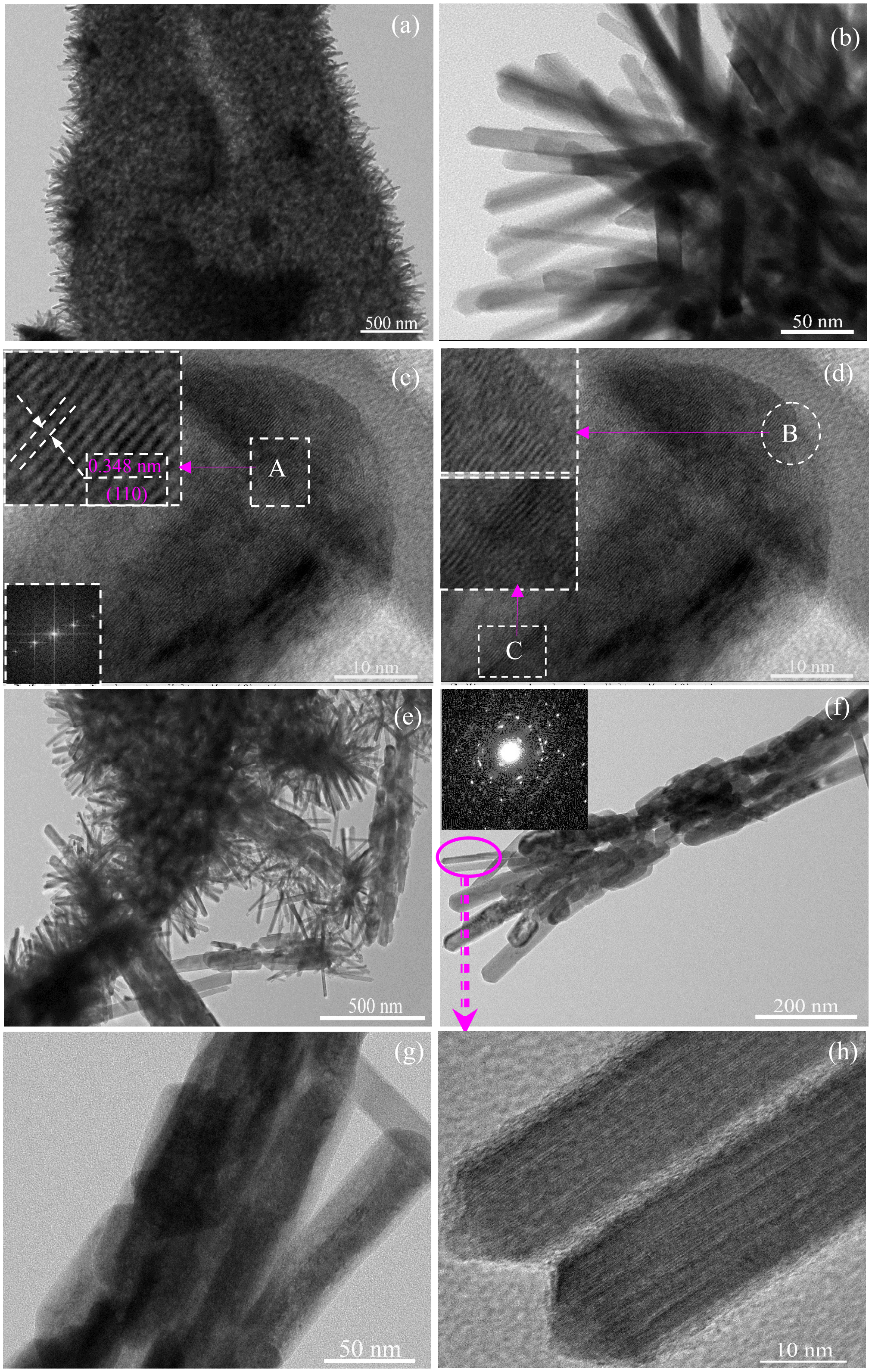

Fig. 3. TEM images of 3 at% Nd-doped SnO_2 nanorod array. (a) TEM image of a section removed from the nanorods arrays at low magnification. (b) TEM image of top nanorods array. (c) HRTEM image of an individual Nd-doped SnO_2 nanorod. Inset: an enlarge lattice fringes of area A and corresponding FFT pattern of HRTEM image, respectively. (d) Enlarge HRTEM image of the marked area B and C showing distorted and discohered lattice fringes. (e) TEM image of bizarre nanorods. (f) A cluster bizarre nanorods at low magnification. Inset: corresponding SAED pattern of the bizarre nanorod. (g) A cluster bizarre nanorods at high magnification. (h) HRTEM image of double nanorods lablled in Fig. b showing unclear, uniform and undulate lattice fringes.

Moreover, it is very valuable that some bizarre nanorods are observed in Fig. 3e. Fig. 3f shows a cluster bizarre nanorods at low magnification. It can be observed that the cluster nanorods were assembled by nanorods with rough surface. The inset shows the corresponding SAED pattern of the individual nanorod, which is made up of the different diffraction discohered circles, indicating that the bizarre nanorods is polycrystalline. The enlarge TEM image of a bizarre nanorod assembly shown in Fig. 3g demonstrates that the SnO_2 nanorods was constructed by rods-like or elliptical grain structure with rough surface. In addition, a corresponding HRTEM image of two parallel nanorods which was marked in Fig. 3f was shown in Fig. 3h. It is quite obvious from Fig. 3h that the lattice fringes of bizarre SnO_2 nanorod are not clear, inconsistent and undulate, suggesting a great quantity of defects in the surface structure of the nanorods. Although the microstructures of these bizarre nanorods needs to be further observed in detail, it is reasonable to suspect that it is the crystalline phases of $Nd_2Sn_2O_7$, since the diffraction peak of $Nd_2Sn_2O_7$ phase was detected in the XRD measurement as shown in Fig. 1.

Raman scattering is an important spectroscopic tool for the characterization of nanometric size effects and a qualitative probe of the presence of lattice defects in solids on vibrational properties. The SnO_2 nanocrystal is rutile in nature and belongs to the space group D_{4h}[14], of which the normal lattice vibration at the Γ point of the Brillouin zone is given on the basis of group theory:[42] $\Gamma = 1A_{1g}(R) + 1A_{2g} + 1B_{1g}(R) + 1B_{2g}(R) + 1E_g(R) + 2A_{2u}(IR) + 2B_{1u} + 4E_u(IR)$. Among them, A_{1g}, B_{1g}, B_{2g} and E_g are the four first-order active Raman modes, the active IR modes are A_{2u}, E_u and B_{1u}, and two silent modes are A_{2g} and B_{1u}, respectively. The Raman spectrum performed at room temperature in the range of 300−900 cm^{-1} of the prepared nanoarrays is shown in Fig. 4. Vibration peaks can be clearly observed at 358.1, 474.1, 578, 631.4, 693.4 and 774.4 cm^{-1}. The most intense peak observed at 631.4 cm^{-1} can be attributed to the A_{1g} mode, while those exhibited at 474.1 and 774.4 cm^{-1} may be due to vibrational modes E_g and B_{2g}, respectively. The A_{1g} and B_{2g} modes are induced by the expansion and contraction vibration mode of Sn–O bonds vibrating in the plane perpendicular to the c-axis, and usually appear in bulk single crystals or polycrystalline SnO_2 materials, whereas the E_g mode may be related to the vibration of oxygen in the oxygen plane vibrating in the direction of the c-axis. These Raman features give evidence that the as-synthesized layered SnO_2 nanoarrays possess the features of the tetragonal rutile structure.[43] Furthermore, the other extra peaks are observed at 358.1, 578, 693.1 cm^{-1} and the observation of these new peaks can be explained on the basis of the nano-effect. In nanocrystalline SnO_2 system, the surface properties are sensitive not only to the grain size and their distribution, but also to the oxygen vacancies and local disorder. Therefore, it is easy to observe the new modes in the Raman spectra.[44] The Raman scattering peaks at 578 and 693.1 cm^{-1}, showing minor shoulder features, might originate from the imperfections of surface structure.[45] The broad peak around 358.1 cm^{-1} which was reported in extra-fine nanoparticles[46] is observed in all samples. It attributes to relaxation of Raman selection rule by a reduction in the particle size or by the high concentration of surface defects such as oxygen vacancies and lattice disorder.[47] In fact, the Nd dopant might be responsible for the changes in local disorder and defects that result in lattice distortion and reduction in lattice space symmetry, which cause many surface defects such as oxygen vacancies and lattice disorder. Another feature to be noted is the intensities of all the Raman peaks are found to decrease in the doped samples. The decrease in intensity suggests that the Nd dopant interacts strongly with the support. The interaction between the Nd^{3+} atoms and the support oxide hinders the crystallization, which is reflected in the reduction of peak intensity. This results supports the observation of XRD and SEM as shown in Fig. 1 and Fig. 2. The Raman spectrum results confirm the characteristics of the tetragonal rutile structure as well as revealing the peculiar features relating surface structure of the Nd-doped SnO_2 layered nanorods array.

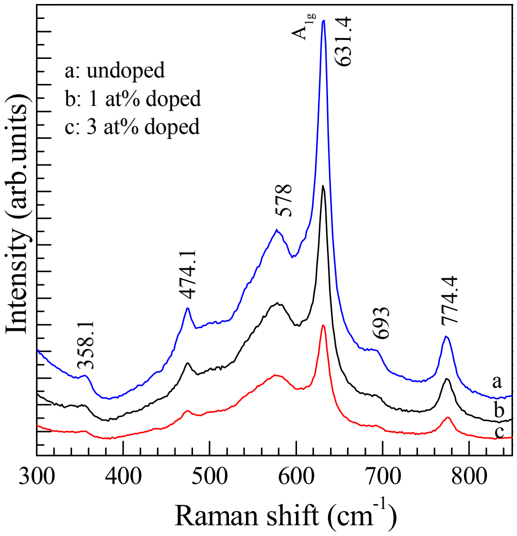

Fig. 4 Raman spectra of Nd-doped l SnO_2 nanorods arrays. a: undpoed. b: 1 at%. c: 3 at%.

XPS is a powerful technique to investigate the chemical composition and the valence state of the elements. The narrow scan XPS spectra were measured in order to study the chemical bond configuration and the composition of as-prepared 3 at% Nd-doped SnO_2 nanoarrays and the result was shown in Fig. 5. The carbon 1s line is used as the energy reference material to calibrate the binding energy scale for XPS measurements and to compensate the surface charging effect. Measured spectra surveys were decomposed into Gaussian components with a Shirley background using the software XPSPEAK. Fig. 5a shows the binding energy of the C1s at 285.16 eV, which might be introduced from the adsorption of the sample surface and the contamination of the instrument. In the present study, the high-resolution XPS spectra survey of Sn 3d (Figure 5b) depicts that Sn $3d_{5/2}$ peaks respectively occur at 487.32 eV, while the Sn $3d_{3/2}$ peak is located at 495.78 eV. The energy difference between Sn $3d_{5/2}$ and Sn $3d_{3/2}$ peak is 8.46 eV, which is in good agreement with the energy splitting reported for SnO_2.[48] Sn $3d_{5/2}$ peak of the prepared SnO_2 nanorods is closely consistent with the standard data (486.70 eV), indicating that Sn is present in a chemical state of +4. The Nd dopant XPS spectra of 3 at% Nd-doped SnO_2 nanoarrays presented in Fig. 5c. It exhibits the energy loss peak is centred at 121.5 eV, which is closely consistent with the standard binding energy of Nd 4d (120.8 eV). XPS results show that Nd is in the +3 oxidation state in Nd-SnO_2.[49] The O 1s spectrum of SnO_2 nanoarrays was presented in Fig. 5d. The broad and asymmetric nature of this peak could be due to various coordinations of oxygen in nanorods. The obtained O1s peak can be Gaussian divided into three symmetrical peaks located at 530.72 eV, 531.13 eV and 532.29 eV, respectively, indicating that there are three kinds of oxygen species in the sample. The low binding energy (530.72 eV) is assigned to O^{2-} ion in the SnO_2 crystal lattice ($O_{lattice}$) under completely oxidized stoichiometric conditions,[50] whereas the binding energy of 531.13 eV can be ascribed to the absorbed O_x^- species (O− or O_2^- ions) in the oxygen deficient regions caused by oxygen vacancy (V_O), oxygen interstitial (O_i) and oxygen antisite (O_{Sn}),[51] which enhance the holes concentration to be helpful to absorb oxygen from the atmosphere.[52] Importantly, the highest peak at 532.29 eV corresponds to chemisorbed and dissociated oxygen species (O^- or O^{2-}) on the surface of Nd-doped SnO_2 nanoarrays,[53,54] suggesting the amount of chemisorbed oxygen increased by the Nd doping. Thus, the increasing number of adsorbed oxygen ions could contribute to gas sensitivity because that the lattice oxygen does not react with the reducing gas.

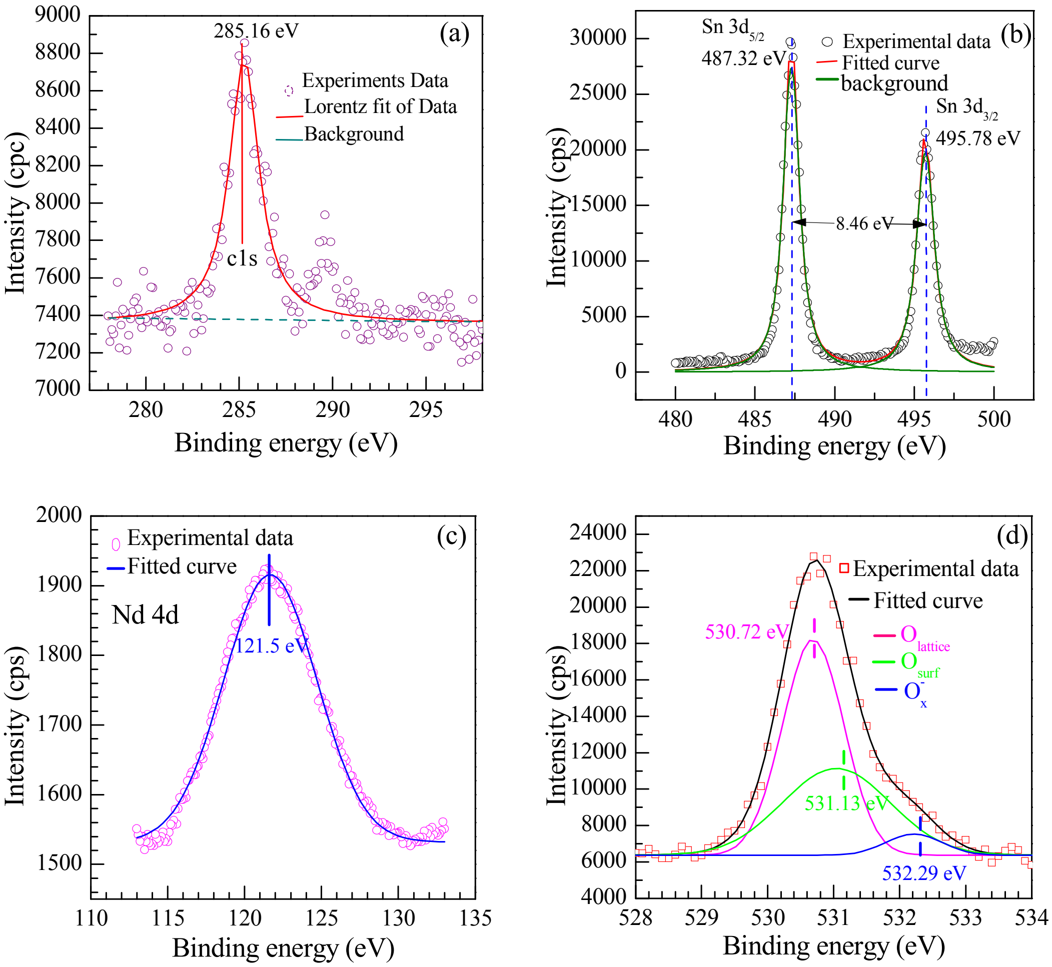

Fig. 5 High-resolution XPS spectra of Nd-doped SnO_2 nanorods array. (a) C1s. (b) Sn3d. (c) O 1s and (d) Nd 4d region.

Brunauer-Emmett-Teller (BET) nitrogen adsorption and desorption measurements of the as-prepared Nd-doped SnO_2 nanorods array product was carried out to predict the sensing performances. The representative N_2 adsorption and desorption isotherm and the corresponding BJH pore size distribution plot of the 3 at% Nd-doped SnO_2 nanorods array was shown in Fig. 6. The isotherm exhibited a hysteresis loop at the p/p_0 ranges of 0.40-0.95 (Fig. 6a), which was associated with the filling and emptying of the 3 at% Nd-doped SnO_2 nanorods arrays by capillary condensation. It implies that the SnO_2 nanorarray sample exhibits a larger pore volume between the nanorods. As shown in Fig. 6b, the pore size distribution of the SnO_2 nanorarray sample showed that a narrow peak appeared in pore size region of 5-120 nm and its top value is located at 21 nm, indicating thinner nanorods of SnO_2 nanorarray, which could make a capacious pore space and a large effective surface area. In fact, the specific surface area of the SnO_2 nanorarray was calculated to be 28.621 m^2g^{-1} by BET method, indicating a large of the active surface among the nanorods of SnO_2 nanorarray. Therefore, it is believed that the sensing performance can be improved by a large number of mass transport channels and a large surface area of Nd-SnO_2 nanorarray.

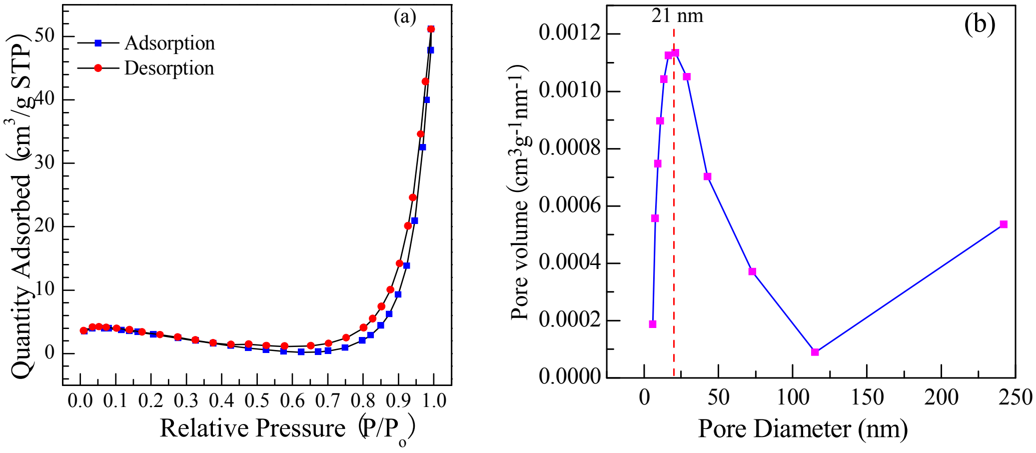

Fig. 6 (a) Typical nitrogen adsorption-desorption isotherm and (b) BJH pore size distribution plots.

3.2. Gas Sensing characteristics of products

Due to the nanorods array structure, the Nd-doped SnO_2 nanorods array may be particularly advantageous for gas sensing applications, and for this reason, we took the pristine and Nd-doped SnO_2 nanoarray products as sensing materials, and investigated the application of the SnO_2 nanoarrays in gas sensor.

It is well accepted that the gas sensitivity is greatly influenced by the amount of dopants and the operating temperature. In order to observe the effects of Nd dopant on the sensitivity of different gases, first of all, we performed the experiments of SnO_2 nanoarray with doping different Nd contents exposed to 200 ppm various testing gases working at an optional operating temperature, 300 °C. The responses of the pristine and doped layered SnO_2 nanorods arrays sensors toward to virous tested VOCs, including alcohol, acetone, toluene, isopropanol, methane, ammonia and so on were shown in Fig. 7. It demonstrates that all the sensors of SnO_2 nanoarray assemblies exhibited a good response to alcohol, isopropanol and acetone, which is in agreement with the previous reports.[27,55] It is more important that the enhanced response to alcohol, isopropanol and acetone is observed after doping a certain amount of Neodymium. In particular, the response improvement to alcohol is very significant. Therefore, the discussions followed are focused on the response to alcohol of Nd-doped SnO_2 nanoarrays.

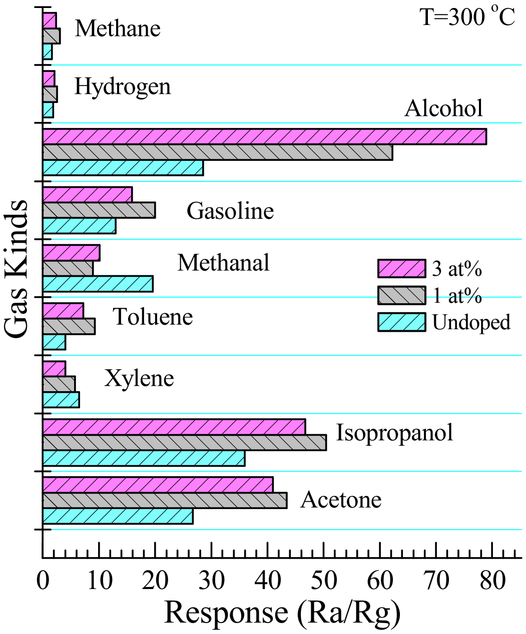

Fig. 7 Response of the Nd-doped SnO_2 nanorods arrays to different kind gases at 300 °C.

Fig. 7 also indicates that an appropriate amount of Nd doping can greatly improve the gas sensing properties of layered SnO_2 nanoarray. It can be seen that the sensor based on 3 at% Nd–doped SnO_2 nanoarray exhibited the highest response to alcohol and the response amplitude was about 78, while the response of the 1 at% Nd–doped SnO_2 nanoarray sensor was 56. However, the highest response of the pristine SnO_2 nanoarray sensor toward 200 ppm alcohol is only 26. The response of the 3 at% Nd–doped SnO_2 nanoarray is more than 3 times larger than that of the pristine SnO_2 nanoarray. This result indicates that the Nd dopant is beneficial to improve the response toward alcohol, and 3 at% Nd is an optimum concentration for getting highest response in our Nd-doped SnO_2 nanoarrays system. The higher responses are probably attributed to their bigger specific surface, which can absorb more oxygen molecules to react with alcohol molecules.

To research the influence of operating temperature and to get an optimum operating temperature, we tested the responses of SnO_2 gas sensors to 200 ppm alcohol as a function of operating temperature and the result was shown in Fig. 8. From the curve, it can be seen that the sensing response first increased, and reached its maximum at a certain temperature, and then rapidly decreased with the increasing temperature. The reason can be explained as follows: an n-type metal oxide can adsorb oxygen from the atmosphere both in the O^{2-} and in the O^{-} species. The adsorption of O^{-} is the most interesting process for sensors because this oxygen ion is the more reactive and thus makes the material more sensitive to the presence of reducing gases. At relatively low temperature of the surface preferentially adsorbs O^{2-} and the sensitivity of the material is consequently very small. As the temperature increases, the dominant process becomes the adsorption of O^{-}, and then the response increases too. If the temperature increases too much, progressive adsorption of all oxygen ionic species previously adsorbed occurs and the response decreases.[56] For the 3 at% Nd-doped SnO_2 nanoarrays, the maximal response to 200 ppm of alcohol vapor was about 136.3 at 260 °C, and then decreased. Thus the optimized operating temperature is determined to be 260 °C. However, it could be found that the optimal working temperature of prinstine and 1 at% Nd-doped SnO_2 nanoarrays was about 310 °C and 266 °C, and the maximal response to 200 ppm of alcohol vapor was only about 36.3 and 98, respectively. It indicates that the 3 at% Nd-doped SnO_2 nanoarrays sensors have a lower optimum temperature and a higher response than that of pure and 1 at% Nd-doped SnO_2 nanoarrays sensors. The reason could be explained on the basis of the change in the energy barrier height and the excellent electrocatalytic effect in due to the doping of 3 at% Neodymium in SnO_2 nanoarrays.[57]

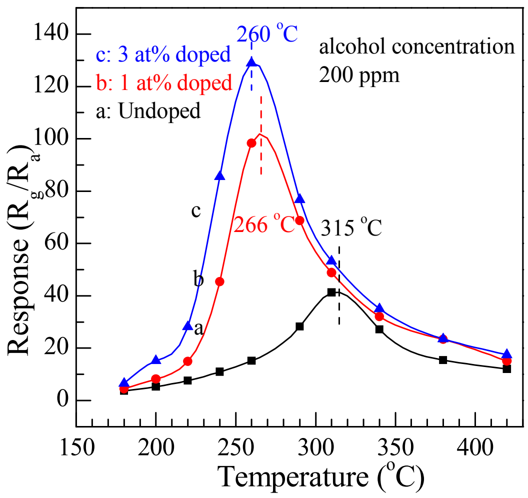

Fig. 8 Gas response depending on the operating temperature of the Nd-doped SnO_2 nanorods array.

A repeatable characteristic and rapid response and recovery to a target gas are demanded for practical application. Fig. 9 shows the representative dynamic gas response of the SnO_2 nanorods array gas sensor to alcohol with concentrations ranging from 1 ppm to 200 ppm when the sensor worked at 260 °C. Six cycles were successively recorded, corresponding to alcohol concentrations of 1, 5, 10, 20, 50, 100, and 200 ppm, respectively. An overview from Fig. 9 was evident that the response amplitude of the sensors gradationally increases with the gas concentration increasing from 1, 5, 10, to 200 ppm. It can be seen from Fig. 9 that the response and recovery characteristics were almost reproducible as well as the quick response and recovery times, indicating a stable and repeatable characteristic and maintaining fast response and recovery state. Particularly, the response and recovery characteristics of the Nd-doped SnO_2 nanoarrys were significantly improved after doping Nd. Noticeably, as shown in the inset of Fig. 9, the sensor presents a considerable response of 7.2 to low alcohol concentration of 1 ppm, and 16.3 to concentration of 5 ppm at the operating temperature of 260 °C, indicating the sensor based on as-prepared SnO_2 nanoarray product is favourable to detect alcohol with low concentration.

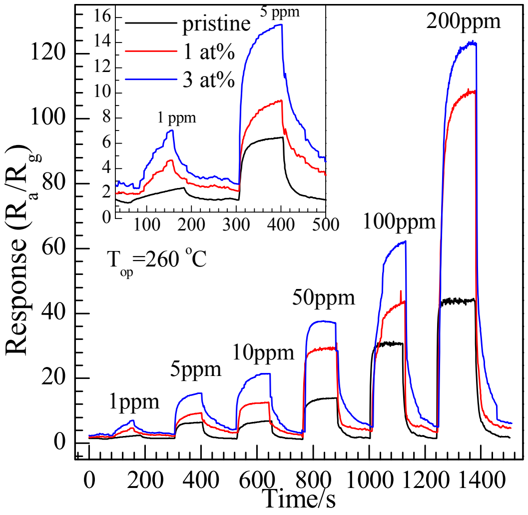

Fig. 9 Dynamic response and recovery behaviors of the Nd-doped SnO_2 nanorods array sensors exposed to different concentrations.

The gas-sensing response and recovery time is an important consideration to evaluate the performance of a gas sensor. Here, we defined as the time required to achieve 80% of the total resistance variation when the gas goes in and out. The time of 80% resistance for gas exposure (t_{on}) and that for recovery (t_{off}) were calculated from the resistance–time data shown in Fig. 10 a and b, which is the response transient of the sensors to 5 ppm and 200 ppm alcohol at 260 °C, respectively. Measured from the curves, in the pristine SnO_2 nanoarrays sensor, it is found that the sensing response and recovery times are 16 s and 38 s for 5 ppm alcohol, 18 s and 43 s for 200 ppm alcohol, respectively. However, in the sensors of 1.0 at% and 3.0 at% Nd-doped nanoarray SnO_2, response and recovery times are about 42 s and 65 s for 5 ppm alcohol, 38 s and 63 s for 200 ppm alcohol, respectively. This result suggests that both the response and recovery become slower after Nd doped, which is in a good agreement with the results reported by G.T. Ang[55] and S.L. Shi.[58] that response and recovery become slower after doped rare earth dopants might take place in the SnO_2 system. The slower response implies the decrease of the chemical reaction rate, resulting the Nd dopant elevate the activation energy of the chemical reaction which will prolong the response and recovery time. Though the detailed origin is not clear yet, and need further investigation, it is evident that the Nd doping caused the response and recovery time prolonged.

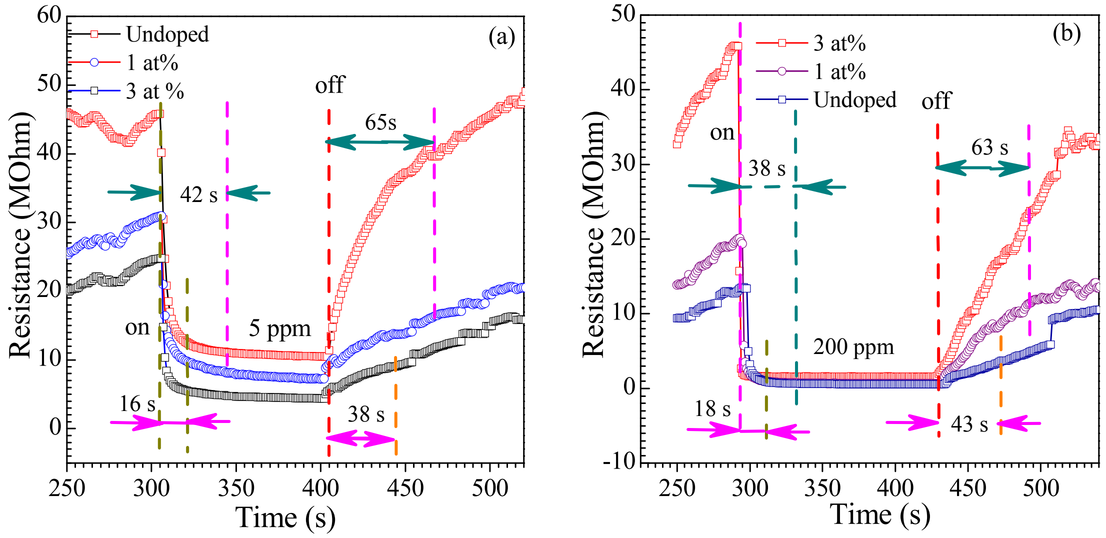

Fig. 10 Response and recovery transient time examined of the pristine and the Nd-doped SnO_2 nanorods arrays sensors. (a) 5 ppm. (b) 200 ppm.

Responses versus alcohol concentration curves of gas sensors manufactured using the pristine and the Nd-doped content with 1.0 and 3.0 at% SnO_2 nanoarray at operating temperature of 260 °C were summarily shown in Fig. 11. It can be observed from Fig. 11 that the responses of all sensors increase with the gas concentrations. Especially, Fig. 11 presents that sensor based on 3.0 at% Nd-doped SnO_2 nanoarray exhibit much higher response to both gases than pristine and Nd-doped content with 1.0 at% nanoarray SnO_2. For alcohol at concentrations of 50, 200, 500, 800, 1000 and 1200 ppm, the most sensitive SnO_2 (3.0 at% Nd-doped SnO_2 nanoarray) sensor responses are 33.4, 127.6, 242.5, 278.2, 287.4 and 293.73, respectively. It was noteworthy that the Nd-doped SnO_2 sensor fabricated in our work exhibits a higher response for alcohol compared with those sensors based on different SnO_2 nanostructures recently reported in the literatures.[27,30, 33,34,36,55]. Moreover, it is obvious that the 3.0 at% SnO_2 nanoarray increase linearly from 10 to 600 ppm. Generally, the gas response of the semiconductor metal-oxide gas sensor can usually be empirically represented as $R=a[C]^b+1$,[59] where [C] is the concentration of the target alcohol vapour, a is a parameter and b is the surface species charge parameter having value of 1 for O^- and 0.5 for O_2^-. At a certain working temperature, the above equation can be rewritten as $\log(R-1)=b\log(C)+\log a$, indicating the linear relationship between R and C in logarithmic forms. From Fig. 11b, the value of b is 0.96 for 3.0 at% Nd-doped nanoarray obtained by leasts squares fitting of response versus alcohol concentration ranged from 10 ppm to 600 ppm in logarithmic scale. It indicates that the sensitivity almost increased linearly with the increase of the alcohol concentration with R-square confidence value above 0.90, suggesting the dominant adsorbed oxygen species at the surface of SnO_2 nanoarrays sensors is O^- ions. This value agrees well with the values reported in the literature on semiconductor metal-oxide sensor.[60]

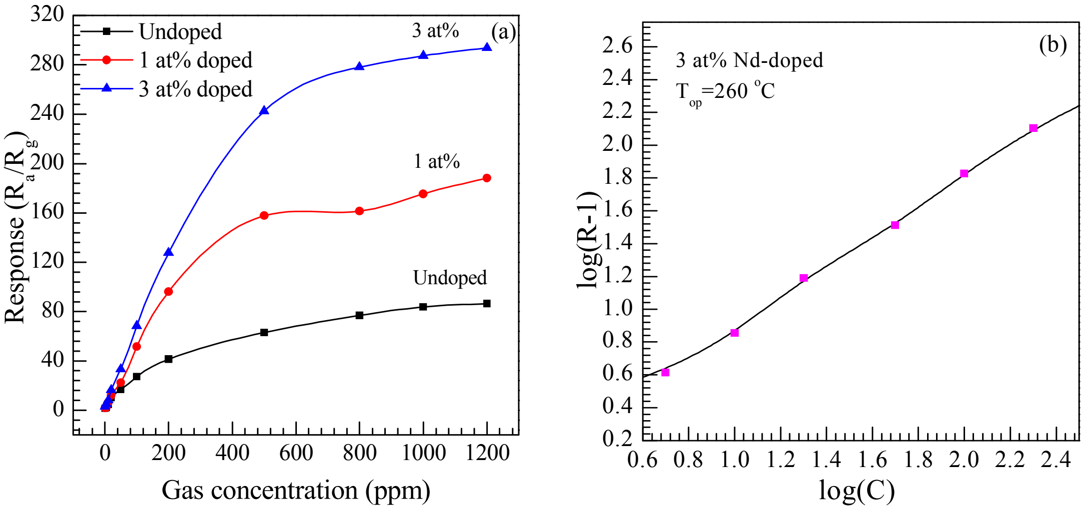

Fig. 11 (a) Gas response to alcohol concentrations. (b) The linear relationship between R and C in logarithmic forms of 3 at% Nd-doped SnO_2 layered nanorods array sensor

In practical application, the long-term stability of gas sensors is critical, for which we must determine the reliability of gas sensors and their length of service. To verify the stability of the of 3 at % Nd doped SnO_2 sensors, the gas response evolution is measured by repeating the response measurement for a number of times under the different concentration (50, 100, 200, 500, 800, 1000 ppm alcohol at 260 °C) for three months. The responses of 3 at% Nd-doped SnO_2 sensor towards alcohol were measured on 10th, 20th, 30th, 40th, 50th, 60th, 70th, 80th, 90th days after the first measurement and the result was shown in Fig. 12. The 10-days-later response is slightly changed ±9.6%, ±10.3%, ±12.6%, ±15.2%, ±13.4% and 14.1% for 50, 100, 200, 500, 800 and 1000 ppm alcohol gas, respectively, illustrating good stability and reliability of sensor material for commercial application. Thus, the Nd doped SnO_2 nanoarray sensors can be used as a promising material for alcohol sensors.

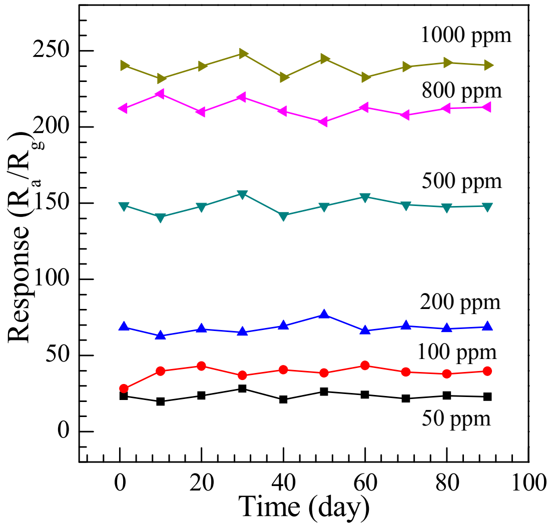

Fig. 12 The stability of the 3 at % Nd-doped SnO_2 nanoarry sensor.

3.3. Sensing Mechanism

As a n-type metal-oxide semiconductor, the most widely accepted theory of tin dioxide (SnO_2) sensing mechanism is built on the change in resistance of the sensor by the adsorption and desorption process of oxygen molecules on the surface of sensing materials.[60,61] As shown in Fig.13, when the SnO_2 nanoarrays sensors are exposed in air ambient, oxygen molecules are chemisorbed and capture electrons from the conduction band of the SnO_2, which induced the formation of an electron depletion layer on the surface of the SnO_2 nanorods and manifested in ordered arrays. It is vital to enhance the receptor function of the sensor and its gas response. Then the chemisorbed oxygen species will be formed by capturing electrons from the conduction band of SnO_2. In this process, oxygen molecules act as electron acceptors only to result in the decrease of electron concentration and the increase of the resistance of the sensor, which can be described by following equations:[61]

$$O_2(gas) \leftrightarrow O_2(ads) \tag{3}$$

$$O_2(ads) + e^- \leftrightarrow O_2^-(ads) \tag{4}$$

$$O_2^-(ads) + e^- \leftrightarrow 2O^-(ads) \tag{5}$$

When the surfaces of the SnO_2 nanoarrays sensors are exposed to reducing gas such as alcohol at a moderate temperature, these gas molecules are oxidized by the adsorbed oxygen species, reducing the coverage of oxygen ions and simultaneously the depleted electrons are fed back into the conductance band of SnO_2, resulting in a narrowed depletion layer and therefore the sensor resistance is decreased. Thus, the conduction in ordered SnO_2 arrays is described by competition between the semiconducting core and resistive shell layers. The reducing gas is oxidized by the reaction with negatively charged surface oxygen, which leads to the increase of conductivity. Alcohol is a reducing gas, which can react with adsorbed oxygen and release the electrons of the oxygen into the conduction band, leading to the decrease of the sensor resistance, thus generating electrical signals. The reaction between alcohol and ionic oxygen species can be described in detail as Eq. (8) and (9).[30] When gas is out, the sensor will be exposed to air again and thus refreshed by air. The sensitivity is based on the surface reaction that takes place between the VOCs with the oxygen ions.

$$C_2H_5OH + 6O^-(ads) \rightarrow 2CO_2 + 3H_2O + 6e^- \tag{8}$$

$$C_2H_5OH + 6O_2^-(ads) \rightarrow 2CO_2 + 3H_2O + 12e^- \tag{9}$$

According to the above reactions, it can be clearly seen that a large specific surface area of the materials can provide more active site for the gas adsorption. Therefore, more electrons are released to reduce the resistance of the materials effectively. As it was confirmed that the large surface area and pore size of nanorods arrays are significantly beneficial for their gas sensing performance,[62,63] the array structure exactly accounts for their better performance than the SnO_2 nanorods structure as the alcohol sensor. In particular, thinner nanorods and densely aligned SnO_2 nanorods of this layered SnO_2 nanorods arrays provide a large surface area, which facilitates the adsorption of oxygen ions and gas molecules on the surface of the material. In addition, the large volume space between the nanorods supported by Fig. 6b is beneficial for gas diffusion and mass transport. These are the explanations for the good performance in alcohol gas sensing, including high sensitivity, fast response and recovery, and low detection concentration limit. The sensing mechanism process of SnO_2 nanorods array for detecting gas is depicted in Fig. 13 a.

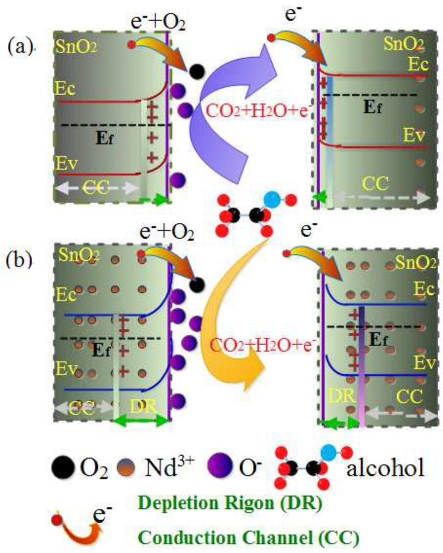

Fig. 13 Schematic illustrations of the gas sensing mechanism of the SnO_2 nanorod array. (a) Undoped SnO_2 nanoarry sensor. (b) Nd-doped SnO_2 nanoarry sensors.

In this work, the response towards alcohol is largely promoted by the Nd dopant. Based on the above gas-sensing results, a possible mechanism of the Nd addition on the gas-sensing properties of SnO_2-based sensors is offered. The improved alcohol response of Nd-doped SnO_2 arrays in this work is attributed to the increase in the amount of absorbed oxygen on the surface of Nd-doped SnO_2 nanorods, which is confirmed by the XPS analysis. The specific surface area is increased with the doping of Nd, which can provide more active sites for gas adsorption on the surface. On the one hand, by doping of Nd, the decrease of crystallite size, which has been proved by XRD and SEM, could lead to the increase of adsorption. Therefore, Nd as an effective grain growth inhibitor that reduced the grain size and hence gave the higher surface area for surface reaction during the detection of alcohol and result in the increase of response. On the other hand, when Nd^{3+} replaces Sn^{4+} in SnO_2 lattice, the incorporating Nd^{3+} ions into the matrix leads more defects such as rougher surface, disordered structures and boundaries (as shown in Fig. 3 and Fig. 4) on the surface of matrix, is conducive to the adsorption of oxygen from the atmosphere,[64,65] which can improve the gas-sensing properties. Thus, a large number of electrons are captured in air and released in alcohol atmosphere, leading a higher response (shown in Fig. 9 and 11). Thus, the sensors based on Nd-doped SnO_2 show a higher response than that of the pure. Moreover, Nd-doped SnO_2 arrays show a better response than the pristine SnO_2 arrays sensors due to the catalytic property of Nd.[37] As one of the high-activity catalysts, Nd dopants can also serve as sensitizers because they are able to increase the amount of active sites on the surface of semiconducting oxides, the detected gases could be easily decomposed. Therefore, Nd doping has a positive effect on gas sensing of nanomaterials. The the enhancement sensing mechanism of Nd-doped SnO_2 nanorods array for detecting gas is schematically depicted in Fig. 13 b.

Finally, it is well known from the above gas sensing results that the level of Nd contents has a significant influence on the response of sensors for alcohol detected. Accordingly, for low concentration of Nd-doped SnO_2 nanoarrays sensors (1.0

at%), the responses were both higher than that of the pristine nanoarrays sensor. With the concentration of Nd increased to 3 at%, the response of 131 to alcohol was much better than 36.3 of undoped thicker nanoarrays sensors, and was still much better than 87.3 of the 1 at% Nd-doped SnO_2 nanoarrays sensors. However, it does not indicate that a high level of doping concentration can cause the better response. This is because redundant doping will reduce the quantity of substituted Nd ions and many clusters such as $Nd_2Sn_2O_7$, Nd-Nd or Nd-O will exist, decreasing the electric transduction of SnO_2 nanoarrays. Then it was the negative effect to improve the gas-sensing properties. Moreover, due to the Nd dopants as one of high-activity catalysts, alcohol molecules could be burned on Nd_2O_3 or $Nd_2Sn_2O_7$ clusters and transformed into CO_2 and H_2O without producing any electric signals.[66] Therefore, only just the appropriate concentration of Nd-doped SnO_2 is propitious to the improvement of gas-sensing properties. Some similar results that only an optimal doping concentration of rare earth is propitious to the improvement of gas sensing properties have been reported in other works.[30,35] According to the above results, it could be calculated that the level of 3.0 at% Nd-doped is an optimal doping concentration and the response is close to the saturated state in our report.

Conclusion

In summary, Nd-doped with different level of SnO_2 layered nanoarrays were fabricated by a facile hydrothermal growth route in the absence of substrates and without any surfactants. The morphology and phase structure results of the Nd-doped SnO_2 nanoarrays investigated by XRD, SEM, TEM, Raman, XPS demonstrated that the Nd-doped layered SnO_2 nanoarray has a hierarchical unique nanostructures combined together by two layers of rutile SnO_2 nanorods with a diameter of 12 nm and length of several hundred nanometers. The Nd-doped nanocomposite SnO_2 nanoarrays kept the crystal structure of the bulk SnO_2 and possesses more surface defects caused by the Nd ions doped into the SnO_2 lattice. The enhanced alcohol-sensing performance of indirect-heating gas sensors based on this unique structure of Nd-doped SnO_2 nanorods arrays indicated that Nd doping greatly improves the gas sensing properties. The Nd-doped SnO_2 layered nanorods arrays with optimized Nd doping level of 3.0 at% exhibited an excellent sensing response toward alcohol at a lower temperature of 260 ^oC. The Nd-doped SnO_2 nanoarray can be used as a promising materiala for alcohol detection, which may have great potential for the development of metal-oxide semiconductor alcohol sensors in environmental gas monitor.

Acknowledgements

This work was supported by the National Natural Science Foundation of China (no. 61161008, 61564009) and the Natural Science Foundation of Yunan Province (2009CD015).

References

1 X. F. Li, X. B. Meng, J. Liu, D. S. Geng and Y. Zhang, *Adv. Funct. Mater*., 2012, **22**, 1647.

2 Y. Fukai, Y. Kondo, S. Mori and E. Suzuki, *Electrochem. Commun*., 2007, **9**, 1439.

3 Y. Zhang, A. Kolmakov, S. Chretien, H. Metiu and M. Moskovits, *Nano Letters*, 2004, **4**, 403.

4 Y. T. Han, X. Wu, Y. L. Ma, L. H. Gong, F. Y. Qu and H. J. Fan, *CrystEngComm*, 2011, **13**, 3506.

5 A. Kolmakov, D. O. Klenov, S. Stemmer and M. Moskovits, *Nano Lett*., 2005, **5**, 667.

6 D. J. Sirbuly, A. Tao, M. Law, R. Fan and P. D. Yang, *Adv. Mater*, 2007, **19**, 61.

7 Z. W. Pan, Z. R. Dai and Z. L. Wang, *Science*, 2001, **291**,1947.

8 X. Y. Kong, Y. Ding, R. S. Yang, Z. L. Wang, *Science*, 2004, **303**, 1348.

9 X. S. Fang, L. M. Wu, L.F. Hu, *Adv. Mater,*. 2011, **23**, 585.

10 G. Z. Shen, J. Xu, X. F. Wang, H. T. Huang, D. Chen, *Adv. Mater*., 2011, **23**, 771.

11 X.B. Li, X.W. Wang, Q. Shen, J. Zheng, W.H. Liu, H. Zhao, F. Yang, H.Q. Yang, *ACS Appl. Mater. Interfaces*, 2013, **8**, 3033.

12 X. Wang, W. Liu, H. Yang, X. Li, N. Li, R. Shi, H. Zhao, J. Yua, *Acta Mater*., 2011, **59,** 1291.

13 K. Zhao, G.F. Du, L. Luo, G.H. Qin, Q.P. Jiang, Y.J. Liu, H.Y. Zhao, *CrystEngComm*, 2015, **17**, 2030..

14 Y. Liu, A. B. Sadik, J. J. Belbruno, M. A. Crane, S. E. Tanski, *Nicotine Tob. Res.*, 2013, **15**, 1511.

15 J. H. Yu, Gy. M. Choi, *Sens. Actuators B*, 2001, **75**, 56.

16 B. Nicolae, S. Markus, G. Wolfgang, *Fresen. J. Analy. Chem*., 1999, **365**, 287.

17 Z.P. Li, Q.Q. Zhao, W.L. Fan, J.H. Zhan, *Nanoscale*, 2011, **3**, 1646.

18 S. Matsushima, T. Maekawal, J. Tamaki, N. Miura, N. Uamazoe, *Chem. Lett.,* 1989, **18**, 845.

19 D. F. Zhang, L. D. Sun, G. Xu, C. H. Yan, *Phys. Chem. Chem. Phys*., 2006, **8**, 4874.

20 L. L. Fields, J.P. Zheng, *Appl. Phys. Lett*., 2006, **88**, 263102.

21 H. Huang, Y. C. Lee, O. K. Tan, W. Zhou, N. Peng, Q. Zhang, *Nanotechnology*, 2009, **20**, 115501.

22 L. Shi, H. L. Lin, *Langmuir*, 2011, **27**, 3977.

23 L. L. Wang, J. N. Deng, Z. Lou, T. Zhang, *J. Mater. Chem. A*, 2014, **2**, 10022.

24 L. L. Wang, T. Fei, Z. Lou, T. Zhang, *ACS Appl. Mater. Interfaces*, 2011, **3**, 4689.

25 J. B. Sun, P. Sun, D. L. Zhang, J. Xu, X. S. Liang, F. M. Liu, G. Y. Lu, *RSC Adv*., 2014, **4**, 43429.

26 J. Wang, F. Yang, X. W. Wei, Y. F. Zhang, L. M. Wei, J. J. Zhang, Q. F. Tang, B. Guo, L. Xu, *Phys. Chem. Chem. Phys*., 2014, **16**, 16711.

27 L. Luo, Q. P. Jiang, G. H. Qin, K. Zhao, G. F. Du, H. Wang, H. Y. Zhao, *Sens. Actuators B*, 2015, **218**, 205.

28 L. L. Wang, H. Dou, Z. Lou, T Zhang, *Nanoscale*, 2013, **5**, 2686.

29 N. S. Murata, T. Y. Suzuki, M. T. Kobayashi, F. K. Togoh, K. K. Asakura, *Phys. Chem. Chem. Phys*., 2013, **15**, 17938.

30 T.T. Wang, S.Y. Ma, L. Cheng, J. Luo, X.H. Jiang, W.X. Jin, *Sens. Actuators B*, 2015, **216**, 212.

31 W. Q. Li, S. Y. Ma, Y. F. Li, X. B. Li, C. Y. Wang, X. H. Yang, L. Cheng, Y. Z. Mao, J. Luo, D. J. Genzang, G. X. Wan, X. L. Xu, *Alloys Comp.*, 2014, **605**, 80.

32 L. P. Chikhale, J. Y. Patil, A. V. Rajgure, F. I. Shaikh, I. S. Mulla, S. S. Suryavanshi, *Ceram. Int.*, 2014, **40**, 2179.

33 F. Pourfayaz, Y. Mortazavi, A. Khodadadi, S. Ajami, *Sens. Actuators B*, 2008, **130**, 625.

34 S. Habibzadeh, A. A. Khodadadi, Y. Mortazavi, *Sens. Actuators B*, 2010, **144**, 131.

35 Y. L. Cao, W. Y. Pan, Y. Zong, D. Z. Jia, *Sens. Actuators B*, 2009, **138**, 480.

36 S. D. Wu, C. Li, W. Wei, H. X. Wang, Y. L. Song, Y.Q. Zhu, L. Z. Lu, *J. Rare Earths*, 2010, **28**, 171.

37 C. Su, Y. C. Zou, X. F. Xu, L. Liu, Z. Liu, L. L. Liu, *Colloids and Surfaces A: Physicochem. Eng. Aspects*, 2015, **472**, 63.

38 Y. L. Wang, M. Guo, M. Zhang, X. D. Wang, *CrystEngComm*, 2010, **12**, 4024.

39 I.T. Weber, A. Valentini, L.F.D. Probst, E. Longo, E.R. Leite, *Mater. Lett.*, 2008, **62**, 1677.

40 X. Ya, G. Z. Zhang, S. P. Zhang, D. W. Zeng, C. S. Xie, *Mater. Res. Bull.*, 2014, **52**, 56.

41 J. Oviedo, M. J. Gillan, *Surf. Sci.*, 2000, **463**, 93.

42 L. Abello, B. Bochu, A. Gaskov, S. Koudryavtseva, G. Lucazeau and M. Roumyantseva, *J. Solid State Chem.*, 1998, **135**, 78.

43 J. F. Scott, *J. Chem. Phys.*, 1970, **53**, 852.

44 D. L. Hou, H. J. Meng, L. Y. Jia, X. J. Ye, H. J. Zhou, X. L. Li, *Phys. Lett. A*, 2007, **364**, 318.

45 D. F. Zhang, L. D. Sun, G. Xu and C. H. Yan, *Phys. Chem. Chem. Phys.*, 2006, **8**, 4874.

46 C. H. Shek, G. M. Lin, J. K . L. Lai, *Nanostruct. Mater.*, 1999, **11**, 831.

47 A. Dieguez, A. Ramano-Rodrigues, A. Vila, J.R. Morante, *J. Appl. Phys.*, 2001, **90**, 1550.

48 Z. F. Dai, L. C Jia, G. T. Duan, Y. Li, H. W. Zhang, J. J Wang, J. L. Hu, W. P. Cai, *Chem.-A Eur. J.*, 2013, **19**, 13387.

49 C. D. Wagner, W. M. Riggs, L. E. Davis, Handbook of X-ray Photoelectron Spectroscopy; PerkinElmer: Eden Prairie, MN, 1979.

50 Y. D. Wang, I. Djerdj, M. Antonietti, B. M. Smarsly, *Small*, 2008, **4**, 1656

51 M. S. Yao, F. Ding, Y. B. Cao, P. Hu, J. M. Fan, C. Lu, F. L. Yuan, C. Y. Shi, Y. F. Chen, *Sens. Actuators, B: Chem.*, 2014, **201**, 255.

52 M. Chen, Z. Wang, D. Han, F. Gu, G. Guo, *J. Phys. Chem. C,* 2011, **115**, 12763.

53 J. C. C. Fan, J. B. Goodenough, *J. Appl. Phys.*, 1977, **48**, 3524.

54 L. X. Zhang, J. H. Zhao, H. Q. Lu, L. M. Gong, L. Li, J. F. Zheng, Sens. *Actuators, B*, 2011, **160**, 364.

55 G. T. Ang, G. H. Toh, M. Z. A. Bakar, A. Z. Abdullah, M. R. Othman, *Proc. Saf. Environ. Protect.*, 2011, **89**, 186.

56 N. Yamazoe, J. Fuchigama, M. Kishikawa, T. Seiyama, *Surf. Sci.*, 1979, **86**, 335.

57 J. Kaur, S. C. Roy, M. C. Bhatnagar, *Sens. Actuators B*, 2007, **123**, 1090.

58 S. L. Shi, Y. G. Liu, Y. J. Chen, J. Y. Zhang, Y. G. Wang, T. H. Wang, *Sens. Actuators B*, 2009, **140**, 426.

59 D. E. Williams, *Sens. Actuators B*, 1999, **57**, 1.

60 N. Yamazoe, G. Sakai, K. Shimanoe, *Catal. Surv.Asia*, 2003, **7**, 63.

61 M. T. Batzill, U. R Diebold, *Phys. Chem. Chem. Phys.*, 2007, **9**, 2307.

62 Z. Y. Zhang, R. J. Zou, G. S. Song, L. Yu, Z. G. Chen and J. Q. Hu, *J. Mater. Chem.*, 2011, **21**, 17360.

63 H. K. Wang, F. Fu, F. H. Zhang, H. E. Wang, S. V. Kershaw, J. Q. Xu, S. G. Sun, A. L. Rogach, *J. Mater. Chem.*, 2012, **22**, 2140.

64 S. Q. Tian, Y. P. Zhang, D. W. Zeng, H. Wang, N. Li, C. S. Xie, C. X. Pan, X. J Zhao, *Phys. Chem. Chem. Phys.*, 2015,

17, 27437.

65 W. An, X. Wu, X. C. Zeng, *J. Phys. Chem. C*, 2008, **112**, 5747.

66 J. C. Belmonte, J. Manzano, J. Arbiol, A. Cirera, J. Puigorbe, A. Vila, N. Sabate, I. Cracia, C. Cane, J. R. Morante, *Sens. Actuators B*, 2006, **114**, 881.